JOURNAL OF COMPUTATIONAL PHYSICS **125,** 464–476 (1996)
ARTICLE NO. 0108

A Spectral Embedding Method Applied to the Advection–Diffusion Equation

M. ELGHAOUI AND R. PASQUETTI

Laboratoire J. A. Dieudonné, URA CNRS 168, UNSA, Parc Valrose, 06108 Nice, cedex 2, France

Received February 27, 1995; revised September 25, 1995

In order to solve partial differential equations in complex geometries with a spectral type method, one describes an embedding approach which essentially makes use of Fourier expansions and boundary integral equations. For the advection–diffusion equation, the method is based on an efficient "Helmholtz solver," the accuracy of which is tested by considering 1D and 2D Helmholtz-like problems. Finally, the capabilities of the method are pointed out by considering a 2D advection–diffusion problem in a hexagonal geometry. © 1996 Academic Press, Inc.

1. INTRODUCTION

As is well known, geometries of complex shape are still difficult to handle, especially for 3D problems, even with the help of automatic mesh generators of structured or unstructured grids. As an example, let us mention the numerical computation of heat transfer in moulds, where the geometries are generally very complex (see, e.g., [1]). This is the reason why, for about 25 years it has been considered that embedding methods can give a satisfying alternative way for handling complex domains (see, e.g., [2]).

Let us recall that the basic idea is to solve a given partial differential equation (PDE) in a simple cartesian domain ω in which the complex domain Ω is embedded. Such approaches, known as fictitious domain methods [3], mask methods [4], etc. have been applied to different kinds of PDE, such as linear elliptic equations but, also, in fluid dynamics to the Euler or Navier–Stokes equations, or in electromagnetism to the Maxwell equations [5–7]. To our knowledge, the closest approaches to the one described in this paper were presented, in a different context, in [8, 9]. In these references, devoted to the development of the boundary element method, the authors handle the body force term by using a Fourier expansion in a larger cartesian domain.

Embedding methods should be especially interesting when combined with spectral methods (Fourier analysis, wavelets, etc.), since the high accuracy of spectral methods is currently reserved for simple geometries. But the preservation of the high accuracy feature, which is not addressed in [8, 9], is generally not trivial, because embedding methods usually produce solutions in ω that are poorly regular at the boundary of the complex domain Ω, thus inducing Gibbs phenomenon.

The goal of this study is to produce a highly accurate embedding method, applicable to conservation equations such as the unsteady advection–diffusion equation or the unsteady incompressible Navier–Stokes equations (spectral methods are not well adapted to the compressible Navier–Stokes equations, due to the possibility of shocks). When using some appropriate finite difference semi-implicit scheme in time, this requires accurate procedures for the solution of elliptic linear problems. This can be achieved by the proposed embedding method, which is based on a combination of Fourier approximations and boundary integral equations. Essentially, this results in the use of two independent meshes, a regular and structured mesh for the simple cartesian geometry, and a boundary element mesh for the complex domain. Moreover, one can say that the method is highly vectorizable or/and parallelizable.

The paper is composed of four main parts (Sections 2–5). In Section 2 we present the basic principles of the approach, by focusing on the unsteady advection–diffusion equation. Then, the details of the method are described in Section 3, concerning the Fourier analysis, and in Section 4, concerning the boundary element approach. Finally, in Section 5, we produce some numerical tests in order to give measurements of the accuracy of the method and to outline its capabilities.

2. DESCRIPTION OF THE METHOD

In a complex (i.e., non-simply connected, non-convex) bounded 2D or 3D domain Ω of boundary Γ, let us consider the following unsteady advection–diffusion problem, in dimensionless form:

0021-9991/96 $18.00

$$\begin{aligned} \partial_t u + v \cdot \nabla u &= \frac{1}{\mathrm{Pe}} \Delta u + g \\ u(t=0) &= u_0 \\ u|_\Gamma &= u_\Gamma, \end{aligned} \tag{1}$$

where the different variables stand for

t, time,
Pe, Peclet number,
g, given time and space dependent body force term,
v, velocity vector, which can be time and space dependent or a function of u, e.g., from the Navier–Stokes equations,
u_0, space dependent initial condition.

For the sake of simplicity, the boundary conditions are assumed to be of Dirichlet type, but as outlined later in the text, all kinds of linear boundary conditions can in fact be treated.

Discretization in time. An efficient way to handle the PDE (1) is to use a finite difference implicit or semi-implicit scheme for the linear terms and an explicit one for the convective term. This yields, at each time-step, the linear elliptic problem

$$\begin{aligned} \Delta u^{n+1} - \sigma u^{n+1} &= f^{n+1} \\ u^{n+1}|_\Gamma &= u_\Gamma^{n+1}, \end{aligned} \tag{2}$$

where the superscript is the time index. For instance, when using, as in Section 5, a second-order backward Euler–Adams–Bashforth scheme, one obtains

$$\sigma = \frac{3\mathrm{Pe}}{2\tau}, \quad f^{n+1} = \mathrm{Pe}\left[\frac{-4u^n + u^{n-1}}{2\tau} + 2(v \cdot \nabla u)^n - (v \cdot \nabla u)^{n-1} - g^{n+1}\right]. \tag{3}$$

The goal is first to produce an efficient solver of Eq. (2), for which the time index is dropped hereafter.

The present embedding method is based on the idea of using the Fourier approximation, to handle the body force term f, and a boundary element approach to force the boundary conditions. This splitting makes use of the linearity of Eq. (2).

As shown in Fig. 1, the domain Ω is now embedded in a simple cartesian domain ω. The algorithm is the following:

(1) In Ω, compute the source term f;

(2) In ω, look for a periodic function $\tilde{f}$ such that $\tilde{f}|_\Omega = f$ ($\tilde{f}|_\Omega$ stands for the restriction of $\tilde{f}$ to the domain Ω);

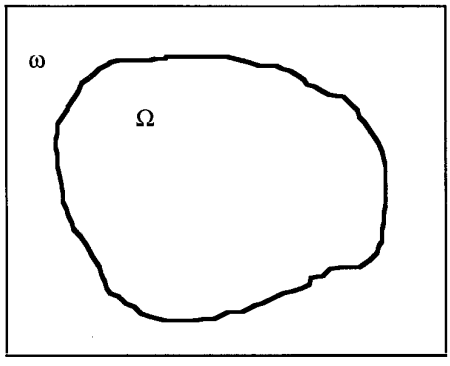

FIG. 1. Embedding method principle.

(3) In ω, determine the Fourier approximation of the periodic solution $\tilde{u}$ of: $\Delta\tilde{u} - \sigma\tilde{u} = \tilde{f}$.

(4) In Ω, using a boundary element approach, solve: $\Delta v - \sigma v = 0$, $v|_\Gamma = u_\Gamma - \tilde{u}|_\Gamma$.

(5) Superimpose $\tilde{u}$ and v: $u = \tilde{u} + v$.

Let us remark that in the case of Neumann boundary conditions one has simply to modify point (4) with the boundary condition: $\partial_n v|_\Gamma = (\partial_n u)_\Gamma - \partial_n \tilde{u}|_\Gamma$.

Section 3 is devoted to points (2) and (3) of the algorithm while in Section 4 we focus on point (4). Point (1), which is also not trivial because it involves the computation of the gradient of u, is also considered in Section 4.

3. FOURIER PART OF THE ALGORITHM

The main point here is to produce the periodic function $\tilde{f}$ such as $\tilde{f}|_\Omega = f$. This function $\tilde{f}$ must be as smooth as possible in order to preserve, as much as possible, the spectral accuracy of the Fourier solution $\tilde{u}$ of the periodic problem. For instance, the extension of f by the zero function would induce a C^0 discontinuity of $\tilde{f}$ and, consequently, a second-order accuracy of the solution, instead of the spectral accuracy.

3.1. *One-Dimensional Analysis*

For the sake of simplicity, let us first assume that the problem is 1D, and introduce a regular cartesian mesh of $\omega =]0, L[$, such as $\{x_i = ih\}$, $0 \le i \le I-1$; $h = L/I$. Using the discrete Fourier expansion, in order to force the periodicity, $\tilde{f}$ may be written

$$\tilde{f}(x_i) = \sum_{k=-I/2+1}^{k=I/2} \hat{\tilde{f}}_k e^{\mathrm{i}kX_i}, \quad \mathrm{i}^2 = -1, 0 \le i \le I-1, \tag{4}$$

where X_i is the reduced value of x_i: $X_i = 2\pi x_i/L$. Introducing the real and complex vectors $\tilde{\mathbf{f}}$ and $\hat{\tilde{\mathbf{f}}}$, whose compo-

nents are the $\tilde{f}(x_i)$ and the $\hat{\tilde{f}}_k$, expression (4) yields the matrix relation:

$$\tilde{\mathbf{f}} = F\hat{\tilde{\mathbf{f}}}, \quad F_{ik} = e^{\mathrm{i}kX_i}. \tag{5}$$

The $I \times I$ complex matrix F can be partitioned into F_1 and F_2, according to whether the collocation points belong to Ω or $\omega\backslash\Omega$:

$$F = \begin{bmatrix} F_1 \\ F_2 \end{bmatrix}. \tag{6}$$

Then the extension problem reads, with the vector $\mathbf{f}$ of the $f(x_i)$:

$$F_1\hat{\tilde{\mathbf{f}}} = \mathbf{f}. \tag{7}$$

Such a problem is clearly underdetermined, but this is not surprising since the extension is not unique.

One simple way to proceed, in order to recover the uniqueness, is to set to zero the highest Fourier modes of $\tilde{f}$. In physical space, such an approach is equivalent to using trigonometric interpolation polynomials defined only with the mesh points interior to Ω. It has been checked that this approach is only satisfactory if the variations of the function f are very smooth. In the case of a stiff gradient of f inside Ω, one observes very large values for $\tilde{f}$ in $\omega\backslash\Omega$.

The classical way to proceed with underdetermined systems like (7) is to introduce a constrained optimization problem, where the functional to be minimized is generally associated with a norm or semi-norm of the solution. The point is then to make an appropriate choice of such a functional, thus leading to (i) a satisfactory result and (ii) an efficient algorithm. Moreover, this choice must not be restricted to the 1D geometry. Coming back to the multidimensional geometry, the algorithm used hereafter to produce a ''regular'' extension is based on the constrained optimization problem

$$\min|\Delta^p\tilde{f}|_{L^2_{\mathrm{per}}(\omega)}, \quad \tilde{f}|_\Omega = f, \tag{8}$$

where Δ is the Laplacian operator and $L^2_{\mathrm{per}}(\omega)$ is the space of the square integrable periodic functions in ω. In this expression the parameter p has to be taken as high as possible (from numerical considerations), since the regularity of $\tilde{f}$ is clearly associated with its value. Indeed, from (8), the functional space of $\tilde{f}$ is essentially the Sobolev space $H^{2p}_{\mathrm{per}}(\omega)$ of the square integrable periodic functions of which the derivatives up to degree $2p$ are also square integrable. Thus, with $p = 0$ (and $\Delta^0 = \mathrm{Id}$, Id: identity operator) one recovers in $\omega\backslash\Omega$ the zero function. Moreover, one can show that the continuous solution of the optimization problem (8) solves:

$$\Delta^{2p}\tilde{f} = 0 \quad \text{in } \omega\backslash\Omega.$$

Due to the proportionality of the $L^2_{\mathrm{per}}(\omega)$ norm in physical and Fourier spaces (Parseval identity) in the framework of the 1D situation the optimization problem (8) reads

$$\min|\Lambda^p\hat{\tilde{\mathbf{f}}}|^2, \quad F_1\hat{\tilde{\mathbf{f}}} = \mathbf{f}, \tag{9}$$

where Λ is the real diagonal matrix such as ($K = I/2$):

$$\Lambda = \mathrm{diag}\{(K-1)^2, (K-2)^2, ..., 1, 0, 1, ..., (K-1)^2, K^2\}. \tag{10}$$

At this point, let us produce the classical (but here false) solution of the quadratic optimization problem under linear constraints (9),

$$\hat{\tilde{\mathbf{f}}} = \Lambda^{-2p}F_1^*(F_1\Lambda^{-2p}F_1^*)^{-1}\mathbf{f}, \tag{11}$$

and make the two following remarks:

—solution (11) is not correct because the matrix Λ is not invertible ($\det(\Lambda) = 0$). This difficulty can be overcome, using a two-step analytical development in which the first step is devoted to the determination of the optimal values of the $\hat{\tilde{f}}_k$, $k \neq 0$, and the second step to the determination of the optimal real $\hat{\tilde{f}}_0$.

—solution (11) requires inverting and then handling a very large matrix, within the brackets, since the dimension of this matrix is equal to the number of collocation points inside Ω.

Because of the second remark, which is quite unacceptable in a multidimensional context, one has to produce the right solution in a form where such a matrix does not appear.

Let us introduce the vector $\mathbf{g}$ of the collocation point values of $\tilde{f}$ in $\omega\backslash\Omega$, in such a way that

$$\tilde{\mathbf{f}} = \begin{bmatrix} \mathbf{f} \\ \mathbf{g} \end{bmatrix}. \tag{12}$$

Since the discrete Fourier transform (DFT) is associated with the matrix F^*/I, problem (9) can be written as

$$\min \left| \Lambda^p [F_1^* \; F_2^*] \begin{bmatrix} \mathbf{f} \\ \mathbf{g} \end{bmatrix} \right|^2. \tag{13}$$

The optimal value of vector $\mathbf{g}$ is obtained by setting to 0 the derivative of expression (13) with respect to $\mathbf{g}$. This yields

$$\mathbf{g} = -(F_2\Lambda^{2p}F_2^*)^{-1}F_2\Lambda^{2p}F_1^*\mathbf{f}. \tag{14}$$

Using the DFT of (12) one gets then the Fourier spectrum of $\tilde{f}$.

One observes in Eq. (14) that the matrix Λ is no longer inverted and that the matrix within the brackets is now associated with the external collocation points. Its dimension is thus equal to the number of collocation points in $\omega\backslash\Omega$, which can be assumed small, especially for 1D problems. Concerning the involved calculations, one can express the following remarks:

—the operator F_1^* can be handled by using a DFT of $\mathbf{f}$ extended with the zero function in $\omega\backslash\Omega$.

—the operator Λ^{2p} reduces to a scaling

—the operator F_2 can be handled by using an inverse DFT and then keeping the values at the collocation points out of Ω.

—the matrix in the brackets can be directly expressed,

$$[F_2\Lambda^{2p}F_2^*]_{ij} = \sum_k k^{2p}e^{\mathrm{i}k(X_i - X_j)}, \tag{15}$$

where both x_i and x_j are outside of Ω. Its computation can be made very easy by showing that the matrix element values are all issued from the inverse DFT of the set $\{k^{2p}\}$, $-K + 1 \le k \le K$. Moreover, one can show that this symmetric matrix is positive definite.

3.2. *Multidimensional Analysis*

The previous developments can be easily extended to the nD complex geometries (e.g., multiply connected geometries). For the sake of simplicity, let us focus on the 2D case.

In Eq. (4), one has to substitute to the 1D Fourier expansion the 2D one. Then, in order to get an equation similar to (5), one has to arrange the f collocation point values as well as the associated 2D-spectrum in 1D-vectors. With i_1 ($0 \le i_1 \le I_1 - 1$) and i_2 ($0 \le i_2 \le I_2 - 1$), associated with the x and y directions, this only requires the introduction of a compact bijective relation between indices i such as $0 \le i \le I_1I_2 - 1$ and the index-pairs (i_1, i_2). Similarly, in spectral space, with k_1 ($-K_1 + 1 \le k_1 \le K_1$) and k_2 ($-K_2 + 1 \le k_2 \le K_2$) for the x and y directions, one needs a compact bijective relation between indices k and the index-pairs (k_1, k_2). One that is well suited is

$$\begin{aligned} k &= k_1 + k_2 2K_1; \\ k_2 &= [(k + K_1 - 1)/2K_1], \quad k_1 = k - k_2 2K_1, \end{aligned} \tag{16}$$

where $[\cdot]$ stands for the integer part function. Then in (5), the elements of F read

$$F_{ik} = e^{\mathrm{i}\mathbf{k}\cdot\mathbf{X}_i} \tag{17}$$

with $\mathbf{k}$ for the (k_1, k_2) vector and $\mathbf{X}_i$ for the reduced position vector of point i. Further 2D developments are similar to the 1D ones. The diagonal matrix Λ, defined in (10), now reads

$$\begin{aligned} \Lambda = \mathrm{diag}\{|\mathbf{k}|^2\}, \quad & -K_1 + 1 \le k_1 \le K_1, \\ & -K_2 + 1 \le k_2 \le K_2, \end{aligned} \tag{18}$$

and one has instead of (15)

$$[F_2\Lambda^{2p}F_2^*]_{ij} = \sum_k |\mathbf{k}|^{2p}e^{\mathrm{i}\mathbf{k}\cdot(\mathbf{X}_i - \mathbf{X}_j)}. \tag{19}$$

In the multidimensional context it is again desirable to decrease the dimension of the matrix defined in (19). This can be achieved by fixing the values of $\tilde{f}$ at the external collocation points that are ''away'' from Ω. Then, instead of computing the extension for all the external points one has only to consider the strip of points close to Ω (as shown in Fig. 2). This only requires considering the non-simply connected domain Ω', including both the points of Ω and the points away from Ω, instead of Ω. Then, the dimension of the vector $\mathbf{g}$, in (12), or of the matrix F_2, is lowered to the number of the collocation points of $\omega\backslash\Omega'$.

3.3. *Solution of the Periodic Problem*

In Fourier space the solution to the periodic problem,

$$\Delta\tilde{u} - \sigma\tilde{u} = \tilde{f}, \tag{20}$$

is straightforward, since the Helmholtz operator is then diagonal. In the multidimensional context,

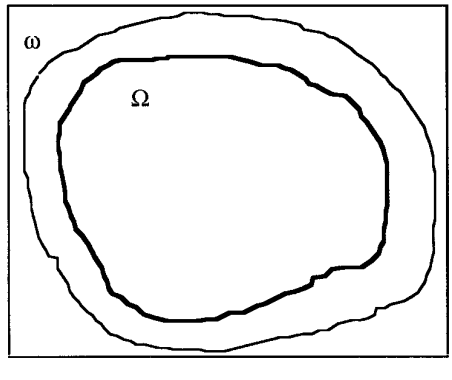

FIG. 2. Continuation strip notion.

$$\hat{\tilde{u}}_k = \hat{\tilde{f}}_k/(-|\mathbf{k}|^2 - \sigma), \tag{21}$$

where again a bijective relation like (16) is used. Moreover, the gradient of $\tilde{u}$ can be easily expressed:

$$\widehat{\nabla \tilde{u}_k} = \begin{bmatrix} ik_1 \hat{\tilde{u}}_k \\ ik_2 \hat{\tilde{u}}_k \end{bmatrix}. \tag{22}$$

It is interesting here to come back to the 1D situation, because the solution of the homogeneous problem (see point 4 of Section 2)

$$\Delta v - \sigma v = 0, \quad v|_\Gamma = u_\Gamma - \tilde{u}|_\Gamma \tag{23}$$

may be written down explicitly. In a domain $]0, \Delta x[$ it reads, with $\sigma' = \sqrt{\sigma}$,

$$v(x) = \frac{v(\Delta x)\sinh(\sigma' x) + v(0)\sinh(\sigma'(\Delta x - x))}{\sinh(\sigma'\,\Delta x)}. \tag{24}$$

Thus, in the 1D situation, one does not need the boundary element solution and one can produce a first test-case for the Helmholtz equation. In Figs. 3a,b,c are given the periodic extension $\tilde{f}$, the periodic solution $\tilde{u}$, and the final solution u for the academic test-case

$$\Omega =]0, \pi[, \quad \omega =]0, 2\pi[, \quad \sigma = 1, \quad u_{\text{exact}} = \cos(x/2),$$

where the boundary conditions and the force term f are derived from the exact solution. These numerical results have been obtained with $p = 1$.

For the highest values of the number of collocation points, the extension of $\tilde{f}$ in $\omega\backslash\Omega$ can be analytically recovered, since with $p = 1$ the continuous solution is such that (see Eq. 9)

$$\Delta^2 \tilde{f} = 0 \quad \text{in } \omega\backslash\Omega; \quad \tilde{f} \text{ in } H^2_{\text{per}}(\omega). \tag{25}$$

For the 1D test problem considered here this implies:

—$\tilde{f}|_{\omega\backslash\Omega}$ is a polynomial of third degree.

—$\tilde{f}$ is C^1 continuous at Γ.

Such a remark can be extended to the cases $p \neq 1$, for which $\tilde{f}|_{\omega\backslash\Omega}$ is a polynomial of degree $(4p - 1)$, C^{2p-1} continuous at Γ.

These considerations are directly connected with the accuracy of the spectral solution. Indeed, it is a classical result from functional analysis that if the source term of a second-order elliptic equation is in $H^{2p}_{\text{per}}(\omega)$, then the solution is in $H^{2p+2}_{\text{per}}(\omega)$, and that the L^2 norm of the error, between the exact solution and its Fourier interpolant, is then decreasing like h^{2p+2} (see, e.g., [10]). Consequently, in the L^2 norm, the accuracy order of the method is equal to $2(p + 1)$. As shown in Fig. 4, for the previous 1D test-case, the order of accuracy is approximatively equal to 4, which is the value obtained with $p = 1$.

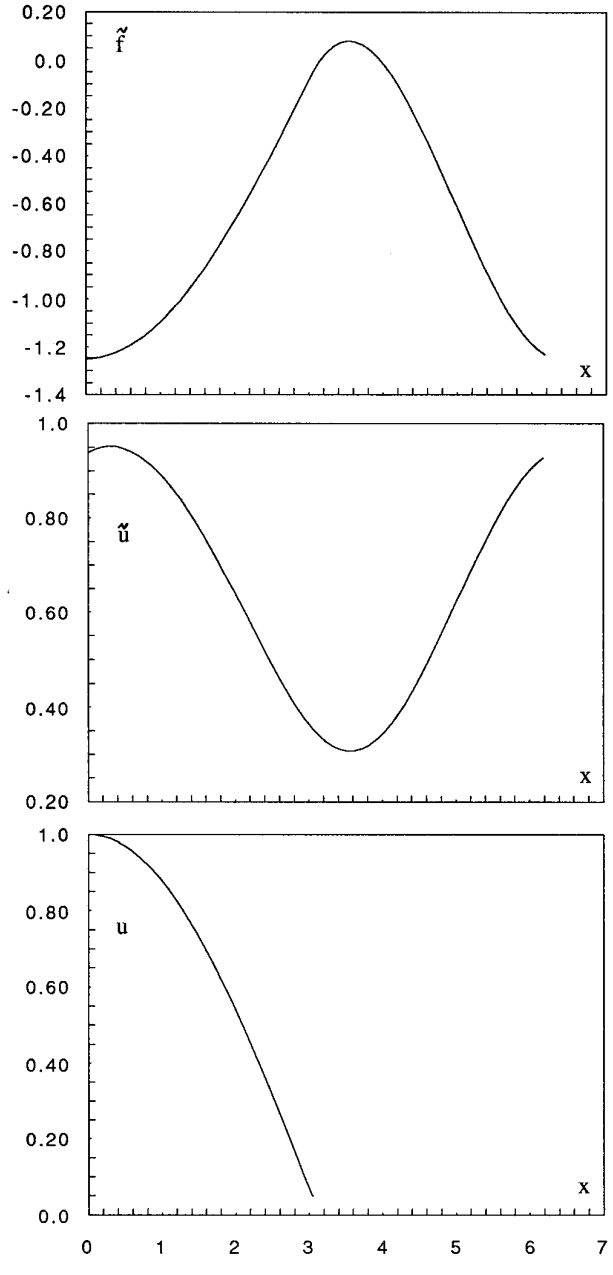

FIG. 3. One-dimensional Helmholtz problem: (a) periodic extended source term; (b) periodic solution; (c) final solution.

4. BOUNDARY ELEMENT PART OF THE ALGORITHM

The aim is now to solve the homogeneous problem (23), for which the solution is not straightforward in the multidi-

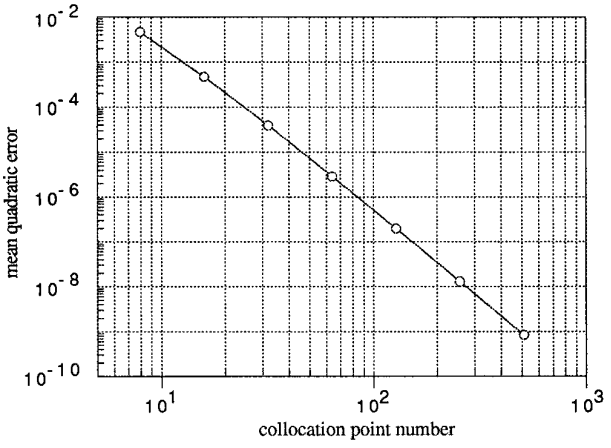

FIG. 4. One-dimensional Helmholtz problem: accuracy of the solution vs the number of collocation points.

mensional context. This can be done efficiently by using a boundary element approach, since Eq. (23) is associated with a boundary integral equation (BIE) involving no domain integral. This BIE reads (see, e.g., [11])

$$c_M v_M + \int_\Gamma v \partial_n v_M^* \, d\Gamma = \int_\Gamma v_M^* \partial_n v \, d\Gamma, \tag{26}$$

where M is a point of $\overline{\Omega}$, c_M is a coefficient equal to 1 if M is in Ω and such that $0 < c_M < 1$ if M is on Γ ($c_M = 0.5$, if Γ is smooth at M), ∂_n is the normal derivative operator. v^* is the fundamental solution of Eq. (23), i.e., a Green function such as in an infinite domain,

$$\Delta v_M^* - \sigma v_M^* + \delta_M = 0. \tag{27}$$

In the 2D case, this Green function reads, with $\sigma' = \sqrt{\sigma}$ and ρ the distance to point M (see, e.g., [12]),

$$v_M^* = +\frac{1}{2\pi} K_0(\sigma' \rho), \tag{28}$$

where K_0 is the modified Bessel function of the second kind and zero order, which presents, for $\rho = 0$, a logarithmic singularity and which exponentially decays at infinity.

Using Eq. (26), the basic principle of the boundary element approach is at first to solve on the boundary and, then, from the boundary values of v and of $\partial_n v$, to compute the internal values.

The discrete form of Eq. (26) is obtained from the discretization of the boundary into boundary elements. Approaches of different approximation orders are then possible, e.g., as done in our 2D code, by using a linear or quadratic approximation for the geometry and a linear approximation for v (2-node Lagrangian elements). But all these methods generally yield a matrix system, for the boundary nodes, of the form

$$(C + H)\mathbf{v} = G\mathbf{q}, \tag{29}$$

where $\mathbf{v}$ and $\mathbf{q}$ are the vectors of the boundary node values of v and $\partial_n v$. With N the number of boundary nodes, C is the $N \times N$ diagonal matrix of the coefficients c_M ($C =$ Id/2 for Lagrangian elements). G and H are geometry dependent $N \times N$ matrices involving boundary integrals of the fundamental solution and of its normal derivative respectively.

At this point, let us mention that the best accuracy of the BEM is obtained when using, instead of local polynomial approximations, global approximations for both the geometry and the function variations, as in [13], where one uses Fourier approximations. Indeed, in this case the approximation order is no longer finite but spectral, as soon as the integrand singularities are analytically removed. In [14], an equivalent result is obtained by removing the singularity of the fundamental solution before using a trapezoidal quadrature method. Unfortunately, such attractive approaches are no longer appropriate when singularities occur, both in the geometry or in the boundary conditions, as is usual in the industrial context. Moreover, handling very complex geometries becomes non-trivial, especially in 3D cases. On the contrary, Lagrangian elements, which are discontinuous elements, are efficient to overcome the singularities and well adapted to the description of complex geometries.

Taking into account the boundary conditions, the usual way to handle a discrete BIE like (29) consists in rearranging all the unknown components of $\mathbf{v}$ and $\mathbf{q}$ in an unknown vector and, then, to solve the resulting $N \times N$ linear algebraic system. When knowing all the boundary values of v and $\partial_n v$, one can compute the internal values of v using the following discrete form of (26):

$$\mathbf{v}' = -H'\mathbf{v} + G'\mathbf{q}, \tag{30}$$

where $\mathbf{v}'$ is the vector of the values of v at N' internal points and H' and G' are $N' \times N$ matrices which only depend on the geometry.

This direct approach was not used for the following reasons:

(i) Equation (30) is not well suited for the computation of the gradient of the solution, which is needed for the computation of the source term of the Helmholtz equation (see (3)). Indeed, the computation of the derivatives of the elements of the matrix H' requires introducing derivatives of each component of the gradient of v^*.

(ii) Equation (30) is not very efficient for the computation of v at the internal points very close to the boundary;

when moving the point M from Ω to Γ, the boundary integral of $\partial_n v^*$ is not continuous, this discontinuity being associated to the jump of the coefficient c_M. This generally results in a less accurate numerical computation of some of the elements of matrix H'.

These remarks lead one to look for a more appropriate formulation. The following "single layer potential" approach [15, 16] yields a satisfactory result.

With $c_M = 0$, the BIE (26) holds outside $\overline{\Omega}$, i.e., in the external domain $\mathbb{R}^n \backslash \overline{\Omega}$ ($n = 2$ in the 2D case). Inversely, by considering the BIE equation obtained when considering this external domain, the following relation holds in Ω:

$$(1 - c_M) v_M - \int_\Gamma v \partial_n v_M^* \, d\Gamma = - \int_\Gamma v_M^* \partial_n v \, d\Gamma. \quad (31)$$

In this equation the coefficient c_M is the one considered in (26) and the fact that the unit outward normal unitary vectors to the boundary of Ω and $\mathbb{R}^n \backslash \overline{\Omega}$ are opposite is taken into account.

From (26) and (31) one gets the "single layer BIE"

$$v_M = - \int_\Gamma v_M^* \mu \, d\Gamma \quad (32)$$

in which μ stands for the jump at Γ of the normal derivative of v.

In discrete form, with $\boldsymbol{\mu}$ for the vector of the jumps at the N nodes, Eq. (32) yields

$$\mathbf{v} = -G\boldsymbol{\mu} \quad (33)$$

for the boundary nodes and

$$\mathbf{v}' = -G'\boldsymbol{\mu} \quad (34)$$

for the internal points. The Dirichlet problem being well posed, matrix G is invertible and so (33) and (34) yield

$$\mathbf{v}' = G' G^{-1} \mathbf{v}. \quad (35)$$

As soon as v is known on the boundary, Eq. (35) is then used to compute all the internal point values. Consequently, in case of Dirichlet conditions one does not need to solve on the boundary, i.e., to compute vector $\mathbf{q}$ as required by (30). Moreover, the computation of the gradient is now simpler since from (32) and (28):

$$\nabla v_M = - \int_\Gamma \frac{\partial v_M^*}{\partial M} \mu \, d\Gamma = \int_\Gamma \nabla v_M^* \mu \, d\Gamma. \quad (36)$$

In discrete form, this leads us to introduce matrices H'_x and H'_y (2D case) that are very similar to the matrix H', since for the computation of their elements one only needs to substitute the unitary basis vectors $\mathbf{e}_x$ and $\mathbf{e}_y$ to the unit outward normal vector $\mathbf{n}$.

Until now the boundary conditions have been assumed to be of Dirichlet type. By solving the problem on the boundary, it is in fact always possible to recover this situation. To this aim, let us consider the general linear boundary condition

$$av + b\partial_n v|_\Gamma = h, \quad (37)$$

where a, b, and h may be space dependent. In discrete form Eq. (37) reads

$$A\mathbf{v} + B\mathbf{q}|_\Gamma = \mathbf{h}, \quad (38)$$

where A and B are two diagonal $N \times N$ matrices of the coefficients a and b at the boundary nodes and $\mathbf{h}$ is the corresponding vector. Combined with (29), (38) yields, with $\mathrm{H} = C + H$,

$$\mathbf{v} = (A + BG^{-1}\mathrm{H})^{-1}\mathbf{h}. \quad (39)$$

5. NUMERICAL TESTS

In order to point out the accuracy of the spectral embedding method, we are going to consider first a 2D Helmholtz equation for which the analytical solution is known. This can be done by choosing a typical solution and then deriving analytically both the body force term and the boundary conditions. Then we will point out the capabilities of the method, by solving a transient advection–diffusion problem.

5.1. *Accuracy of the Method*

The domain that is considered is a hexagon, whose sides are tangent to a circle of diameter 1, centered at the origin. Inside this hexagon, the exact solution reads

$$u_e = \tfrac{1}{4}(1 + \tanh(\alpha x))(1 + \tanh(\alpha y)) \quad (40)$$

in such a way that $0 \leq u_e \leq 1$. The parameter α which controls the stiffness of the solution is taken $\alpha \approx 7.22$ in the calculations.

As shown in Fig. 5, the hexagon is embedded in a square (side ≈ 1.386). In order to decrease the memory storage (see Section 3), the extension is performed in a strip (see Fig. 5). Its thickness is taken equal to a given multiple of the Fourier mesh size.

The following result has been obtained with $\sigma = 1$. In Fig. 6a the function $\tilde{f}$ is shown; in Fig. 6b one has the periodic solution $\tilde{u}$, and in Fig. 6c the numerical solution u, inside the hexagon, is given. The computation has been

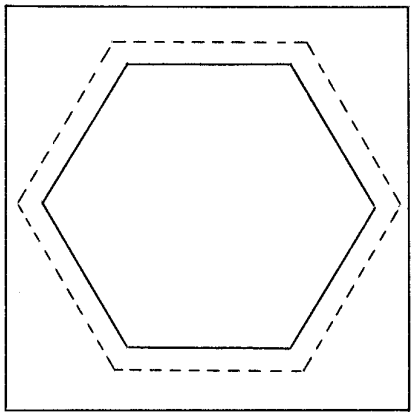

FIG. 5. Schematic of the geometry.

achieved with a $N \times N = 32 \times 32$ Fourier mesh, $N' = 120$ boundary elements, and a 5-step strip for the extension of the source term f. The ratio of the boundary element size to the Fourier mesh size is $r = 0.6875$. For different values of N and N', with the geometry considered in this section, $r = 2.5\ (N + 1)/N'$.

Concerning the computer requirements, one has to discern the preliminary calculations, which are made once, and the solver itself, which will be used at each time step of the unsteady problem. One can mention that on a CRAY YMP the preliminary calculation, which essentially consists in the computation, using a Gauss quadrature method, of regular 1D integrals (routine QDAG of the IMSL, relative accuracy 10^{-6}, maximum number of integration points 21) needs about 650 s and 1.43 Mw of memory storage, whereas the solution of the Helmholtz equation only needs 0.018 s (14% for the extension procedure and 86% for the Fourier–BEM solution) and 1.44 Mw. As could be expected, the major requirements of the method lay in the computation time of the preliminary calculation and in the memory storage, which is already important for a 32×32 Fourier mesh.

Concerning the computation accuracy of this first result, the mean quadratic error between the analytical and numerical solutions is equal to $e_{mq} = 5.3 \times 10^{-6}$, when the mean quadratic value of u_e is equal to 0.414. The maximum error is equal to $e_{max} = 4.9 \times 10^{-5}$ and is located at ($x = 0.563$, $y = 0$). Such a point is very close to the boundary. As discussed later this is due to the boundary element computation, which becomes less accurate when the points of Ω are close to the boundary. This can be confirmed by considering the mean quadratic error obtained for points far from the boundary, e.g., inside a circle centered at the origin and of diameter equal to 0.8. Then one obtains $e'_{mq} = 1.2 \times 10^{-6}$.

In order to go further into this study of accuracy, similar calculations have been performed for different values of

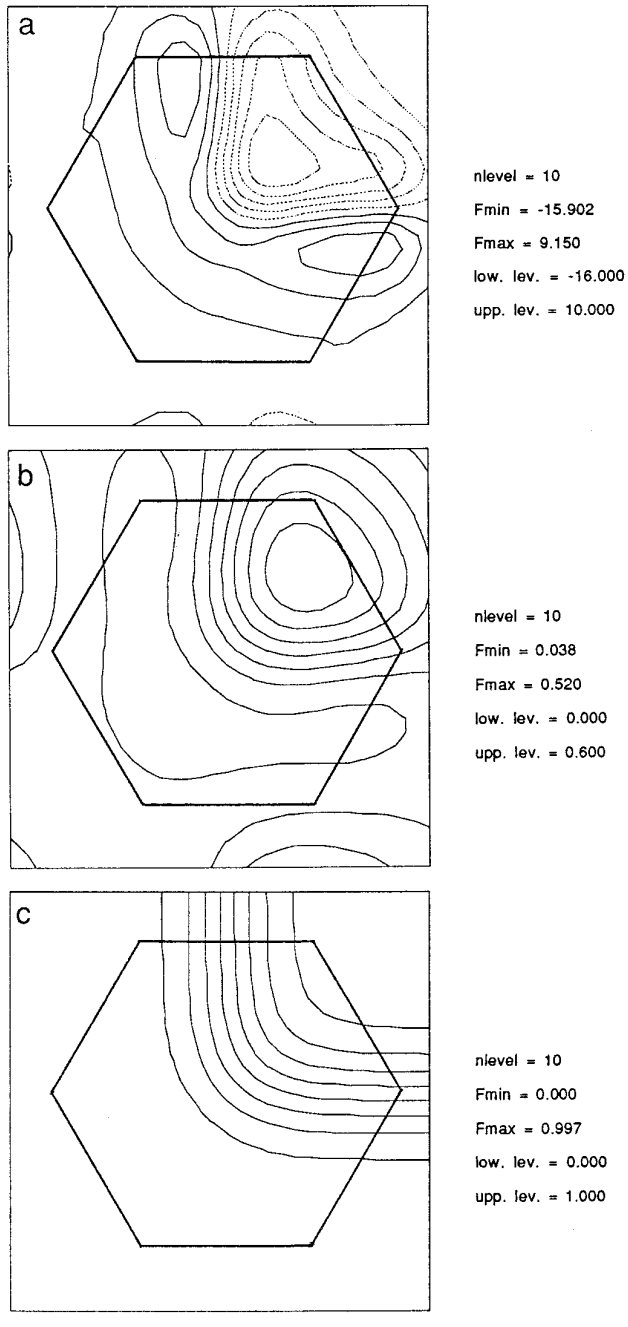

FIG. 6. Two-dimensional Helmholtz problem: (a) periodic extended source term; (b) periodic solution; (c) final solution (extended with the analytical solution (40) outside of Ω).

the parameters N and N'. Such results are summarized in Figs. 7a–b, where $e_{mq}(N)$ and $e'_{mq}(N)$ are given for three different values of N' {30, 60, 120}. It is interesting to observe that each schematic is divided into two regions, which we denote regions I and II. In region I, the mean quadratic errors e_{mq} and e'_{mq} are rapidly decreasing and only depend on N, i.e., on the Fourier mesh, until they

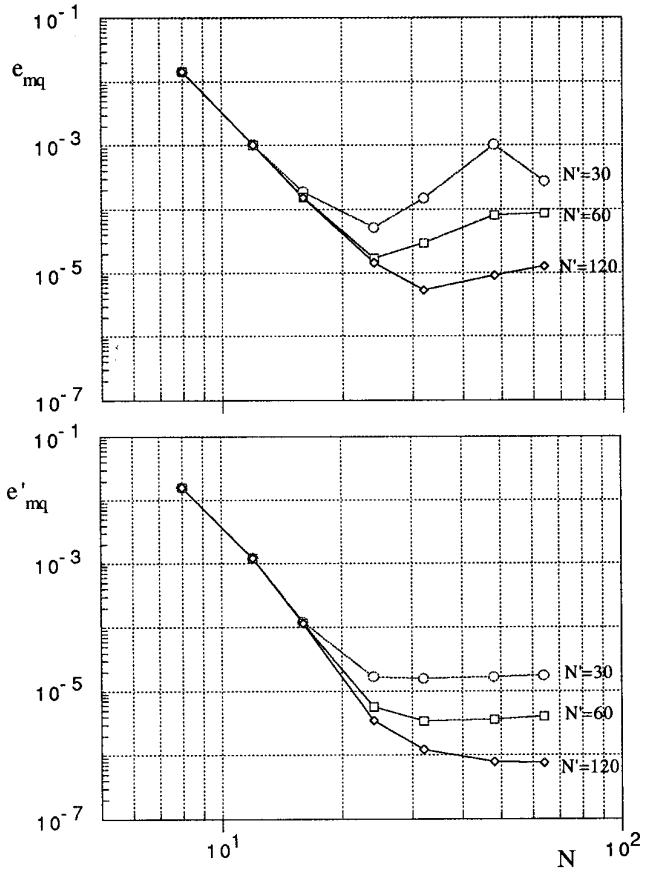

FIG. 7. Two-dimensional Helmholtz problem: accuracy of the solution vs N (for a $N \times N$ Fourier mesh) and for different boundary element numbers N', calculated from (a) all the collocation points or from (b) the collocation points away from the boundary.

reach a limiting value associated with N', i.e., with the boundary element mesh. In region II, e_{mq} is slowly increasing with N from the limiting value defined by N', when e'_{mq} remains nearly constant. Clearly, in region I the accuracy of the method is governed by the Fourier approximation, while in region II it is governed by the boundary element calculation. In region II, the increase of e_{mq} results from the fact that once N is increased the distance between the Fourier colocation points and the boundary is decreased. This can be confirmed by analysing the location of the maximum error e_{max}; these locations and the e_{max} values are given in Table I, for different values of N and for $N' = 120$. Clearly, in region II, for $N = 32$ and $N = 64$, the maximum errors are located near the boundary. It is not the case for $N = 8$ and $N = 16$, which fall into region I.

TABLE I

Maximum Error Values and Locations

N	8	16	32	64
e_{max}	4.3×10^{-2}	8.3×10^{-4}	4.9×10^{-5}	3.2×10^{-4}
x, y	0.173, 0.173	0.087, 0.433	0.563, 0	0.260, 0.500

The sensitivity of the boundary element calculation with respect to the distance to the boundary does not come from a poorly accurate computation of the matrix elements (matrices G and G') associated with the points nearest the boundary. Indeed, all the integrals necessary for constituting the matrices G and G' are computed with similar accuracy (relative accuracy $=10^{-6}$). The difficulty here comes from the fact that this distance can become very small in comparison with the boundary element size. In this case, due to the stiffness of the modified Bessel function of the second kind and zero order (see Eq. (28)) near 0, an accurate calculation at the internal point requires a very accurate solution along the boundary. But this one is not obtained with the Lagrangian linear boundary element, which simply assumes a linear variation of v and $\partial_n v$ (see Section 3). This assumption was also confirmed by the improvements that were obtained when the linear element was substituted for the constant element, which assumes v and $\partial_n v$ are constant along each element. In order to overcome this difficulty one must either increase the approximation order or use more boundary elements. In the two cases, this results in increasing the number of boundary nodes.

For transient calculations, the value of the parameter σ is often high ($\sigma \gg 1$), generally due to the small value of the time-step (see Eq. (3)) required by stability considerations. It is then important to see if the method can support large values for this parameter. To achieve this goal, a study of accuracy similar to the previous one and dealing with the same exact solution (40), was performed for two different values of σ: $\sigma = 10^2$; $\sigma = 10^4$. The number of boundary elements has been taken equal to $N' = 120$.

The results are presented in Figs. 8a,b, where again one can discern regions I and II. In region I, where the accuracy of the periodic solution is dominant, the accuracy is better for the higher values of σ. This is not surprising, since increasing σ tends to produce a more regular source term: $f = \Delta u_e$ if $\sigma = 0$ and $f = -\sigma u_e$ if $\sigma = \infty$. On the contrary, when the boundary element accuracy is dominating in region II, one observes that increasing σ yields a worse accuracy. Moreover, the comparison of e_{mq} and e'_{mq} clearly shows that again the accuracy is lost in the vicinity of the boundary. This stems from the fact that for the support of the fundamental solution becoming very small (see Eq. (28)), an increase in the number N' of boundary elements is needed to improve the accuracy.

All the previous calculations were performed with a 5-step strip for the extension of f. In order to investigate the sensitivity of the method with respect to this parameter, one can produce results obtained (i) with a narrow 3-step strip, (ii) with all the points of $\omega \backslash \Omega$ (∞-step strip), and (iii) with zero for the extension of f in $\omega \backslash \Omega$ (0 step strip).

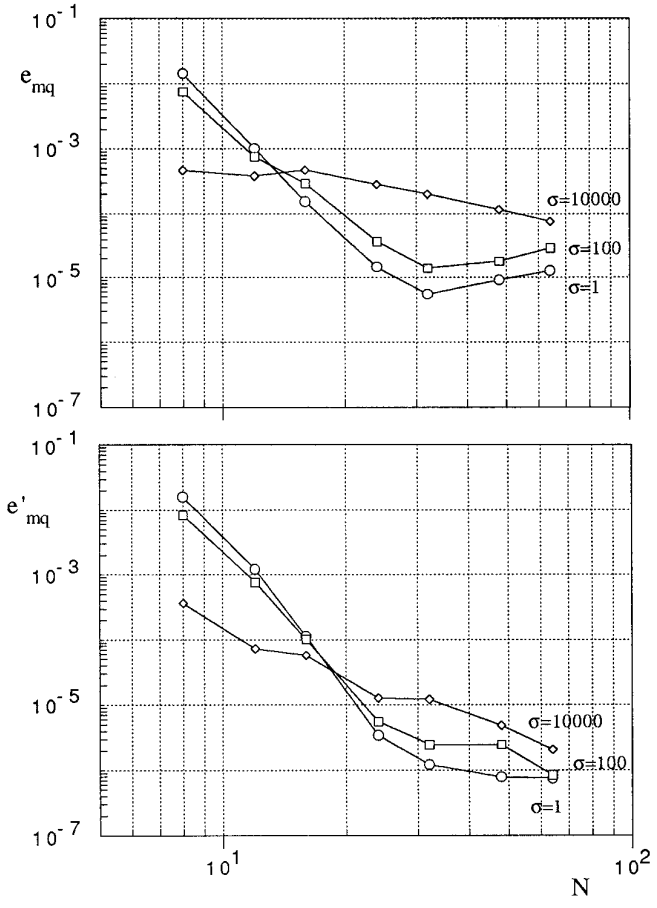

FIG. 8. Two-dimensional Helmholtz problem: accuracy of the solution vs N (for a $N \times N$ Fourier mesh) and for different Helmholtz coefficients, calculated from (a) all the collocation points or from (b) the collocation points away from the boundary.

In Figs. 9a,b the variations of e_{mq} and e'_{mq} with respect to N, $N' = 120$, for the 0-step, the 3-step, the 5-step, and the ∞-step strips, are given. One observes that the results obtained when using the 3-step, the 5-step, and the ∞-step strips are nearly the same. For the smallest values of N, all the results are even identical, because the cartesian domain is then itself embedded in the external hexagon of Fig. 5! In Table II the numbers of collocation points located in the hexagon and in the strip, for these three cases and for different values of N, are given. The second number is equal to the dimension of the matrix defined in (19).

Concerning the 0-step strip, one observes in Fig. 9 that the convergence rate is worse. But for the highest values of N one gets approximately the limiting accuracy, governed by N', obtained with the extension strips.

The previous results were obtained for the Dirichlet problem, which is not the best way to point out the Gibbs phenomenon effect. With Neumann boundary conditions,

TABLE II

Number of Collocation Points inside the Extension Strip

N	8	16	32	64
Inside hexagon	27	111	461	1871
∞-step strip	37	145	563	2225
5-step strip	37	144	434	889
3-step strip	37	124	269	514

the results are given in Figs. 10a–b. The interest of using an extension strip is here obvious. Moreover, one observes that the convergence rate is now smaller and consequently that $N \geq 64$ collocation points are now necessary to reach region II.

This study of accuracy yields the following main conclusions:

—in region I, where the periodic solution accuracy is

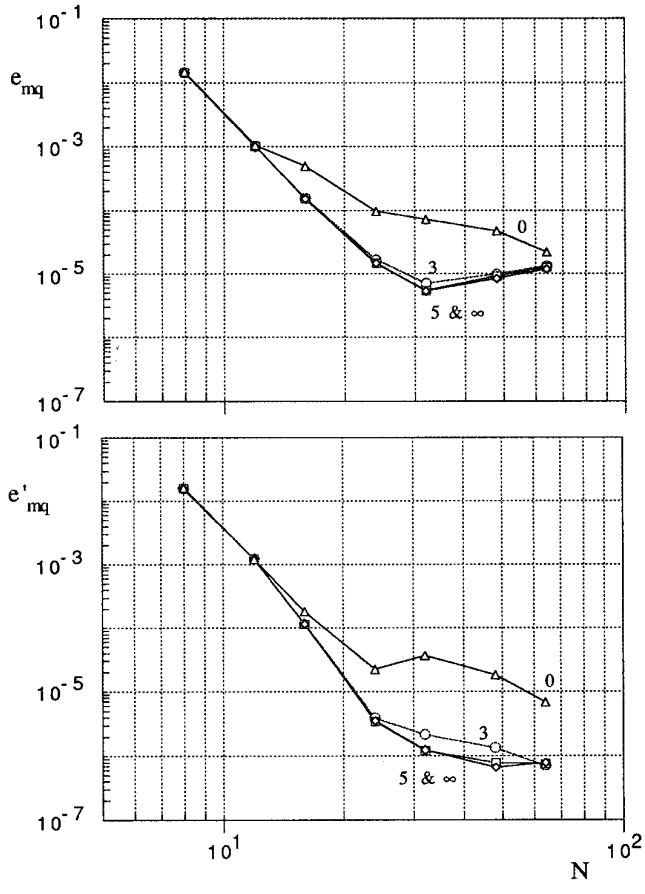

FIG. 9. Two-dimensional Helmholtz problem: accuracy of the solution vs N (for a $N \times N$ Fourier mesh) and for the $\{0, 3, 5, \infty\}$ extension strips, calculated from (a) all the collocation points or from (b) the collocation points away from the boundary.

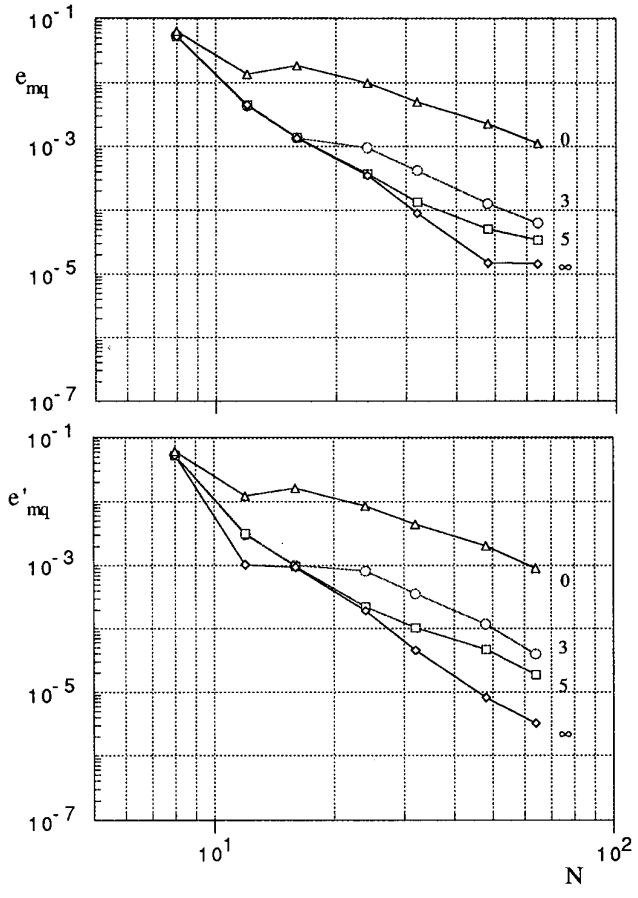

FIG. 10. Two-dimensional Helmholtz problem with Neumann boundary conditions: accuracy of the solution vs N (for a $N \times N$ Fourier mesh) and for the $\{0, 3, 5, \infty\}$ continuation strips, calculated from (a) all the collocation points or from (b) the collocation points away from the boundary.

dominant, the rate of convergence is high. With $\sigma = 1$, it can be estimated greater than 6.4 for the Dirichlet problem and greater than 3.8 for the Neumann problem. This last value is better in agreement with the value of 4 to be expected for calculations done with $p = 1$ (cf. Section 3).

—the boundary element size must be chosen small enough to remain in region I, since in region II an increase of N yields a loss of accuracy. Nevertheless, since increasing N' in region I does not improve the results, it is preferable to use the largest admissible boundary element size, from computing considerations. Unfortunately, determination of the optimal choice of N and N', which depends on σ, is not a trivial task!

—using a narrow strip for the extension is possible. This allows the use of fine $N \times N$ grids for solving the periodic problem, since the dimension of matrix (19) is then small and, approximately, linearly increasing with respect to N.

5.2. *Solution of an Advection–Diffusion Test Problem*

In order to investigate the capabilities of the method, a 2D advection–diffusion transient test problem in the hexagon of Section 5.1 (see Fig. 5) is investigated. To this aim, the semi-implicit second-order scheme defined in Section 2, Eqs. (2) and (3), is used. In order to recover some classical behaviours, the 2D problem is chosen in such a way that its asymptotic solution u_∞ is 1D and:

$$\partial_y u_\infty = \frac{1}{\mathrm{Pe}}\,\partial_{yy} u_\infty, \quad u_\infty(y = -0.5) = 1, \quad u_\infty(y = 0.5) = 0. \tag{41}$$

The analytical solution of this stationary 1D problem is well known:

$$u_\infty = \frac{e^{\mathrm{Pe}(y+0.5)} - e^{\mathrm{Pe}}}{1 - e^{\mathrm{Pe}}}. \tag{42}$$

It is characterized by a boundary layer, at $y = 0.5$, the thickness of which is $O(1/\mathrm{Pe})$.

The transient 2D problem that has been chosen reads:

$$\begin{aligned} &\partial_t u + v.\nabla u = \frac{1}{\mathrm{Pe}}\,\Delta u, \quad v = (0, 1)^t \\ &u(t = 0) = 0 \\ &u|_\Gamma = u_\infty|_\Gamma. \end{aligned} \tag{43}$$

For such a problem $x = 0$ is a symmetry axis, parallel to the direction of the flow. In the half-plane $y < 0$, one has the hexagonal inflow boundary and in $y > 0$, the hexagonal outflow boundary.

The problem was solved for three different values of the Peclet number: $\mathrm{Pe} = \{1, 10, 100\}$. For the computation one has used $N' = 120$ boundary elements, a 128×128 Fourier mesh, and a 5-step extension strip. The time step was taken equal to 5×10^{-3}. Let us also mention that in (43) the gradient results from the superposition of the Fourier and the boundary element components of the solution, from Eqs. (22) and (36).

In Figs. 11a–b to 13a–b, for the different values of the Peclet number, the variations of u at different times (a) along the streamwise symmetry axis $x = 0$ and (b) along the cross-stream $y = 0$ direction are presented. Strong gradients can be observed, especially for the highest values of the Peclet number. They result from (i) the C^0 time discontinuity between the initial condition and the boundary conditions at $t = 0$ and (ii) from the characteristic boundary layer of this advection–diffusion problem. The analytical asymptotic solutions are given by dotted lines and one observes, for the final time values, good agreement between the computed and the analytical profiles. As ex-

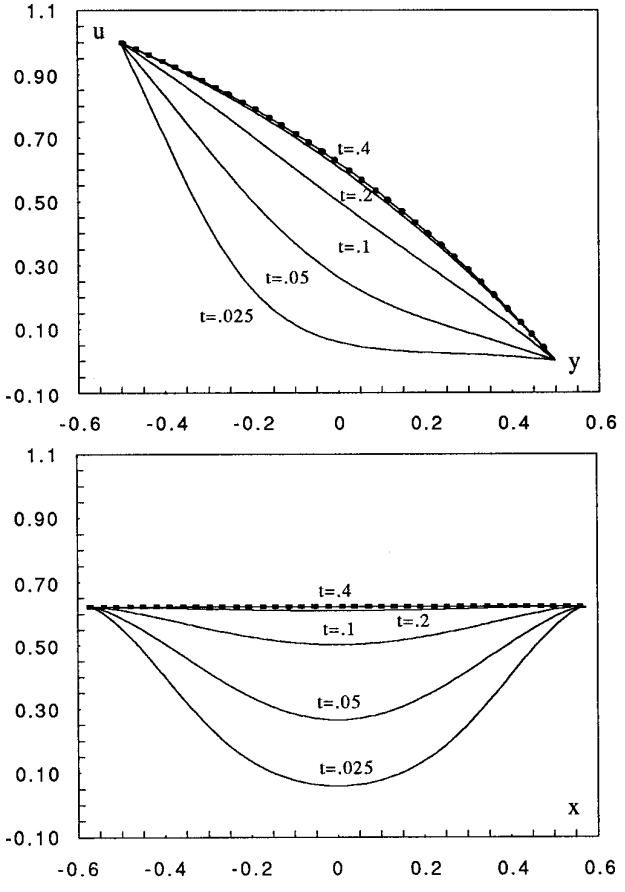

FIG. 11. Advection-diffusion problem, Pe = 1: solution along the axis (a) $x = 0$ and (b) $y = 0$ at different times. Comparison with the asymptotic analytical solution.

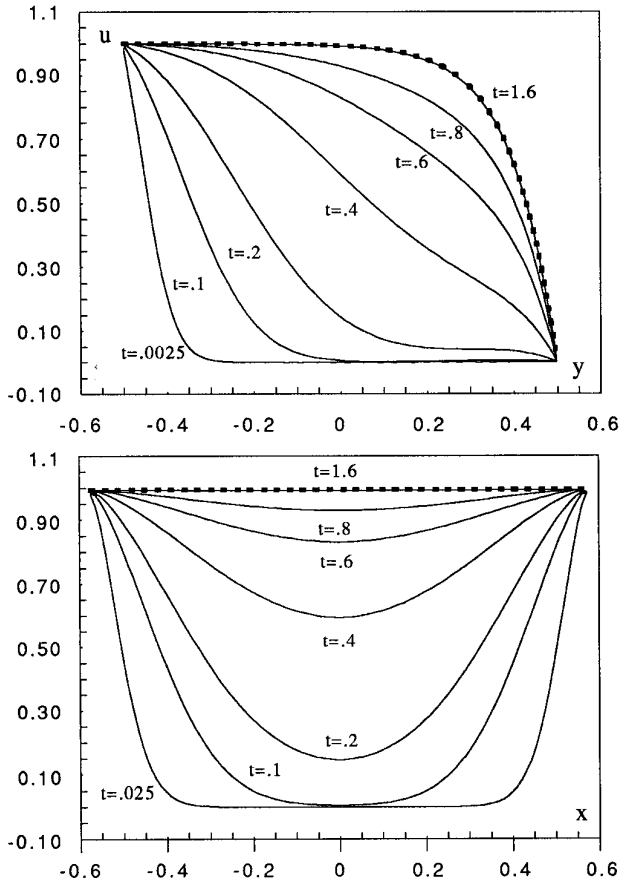

FIG. 12. Advection-diffusion problem, Pe = 10: solution along the axis (a) $x = 0$ and (b) $y = 0$ at different times. Comparison with the asymptotic analytical solution.

pected, when the convective phenomenon is very dominant (Pe = 100) the solution is very stiff, especially in the boundary layer obtained at the final time. But even in this difficult case, one observes that the strong gradients are well computed by the algorithm.

6. CONCLUSION

By focusing on the advection–diffusion equation, a numerical algorithm has been presented for handling in an efficient way the PDE in nD ($1 \leq n \leq 3$) geometry of complex shapes. This spectral embedding method is based on the following ideas:

—using a semi-implicit finite difference scheme in time, in which the linear terms are treated implicitly and the non-linear ones explicitly, in order to produce at each time-step an elliptic linear problem (as is generally done with spectral methods);

—using an embedding approach for handling the body force term, by producing a periodic extension of this body force term, and then by using Fourier analysis to get the periodic solution;

—using boundary elements to enforce the boundary conditions.

In order to obtain a real spectral method, we have been especially interested in developing highly accurate algorithms. Mainly, it has been pointed out that the convergence rate was controlled by the Fourier approximation, until a limiting value associated with the number of boundary elements was found. The accuracy of the spectral solution essentially depends on the regularity of the body force term extension, and so it was at first necessary to develop an efficient extension algorithm. The one presented here yields a regular periodic source term and efficiency is obtained, out of the 1D situation, by using an extension strip. Concerning the boundary element part of the algorithm, it has been focused on the Helmholtz equation which results from the finite difference approximation of the unsteady advection–diffusion equation. The single layer formulation has been used to overcome the classical problem of the

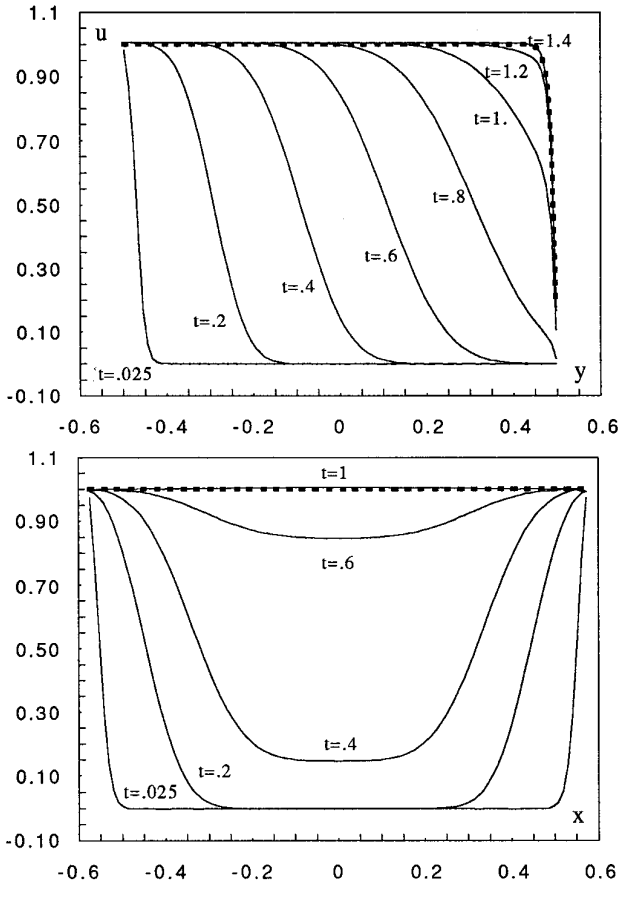

FIG. 13. Advection-diffusion problem, Pe = 100: solution along the axis (a) $x = 0$ and (b) $y = 0$ at different times. Comparison with the asymptotic analytical solution.

jump at the boundary of the integral associated with the normal derivative of the Green function. For 1D and 2D situations, accuracy measurements were performed, in order to point out the high level of the final global accuracy of the approach. Nevertheless, research is still in progress to enhance the convergence rate and the accuracy of the solution in the vicinity of the boundary.

The capabilities of the method have been pointed out by considering a 2D advection–diffusion problem in a hexagon. Calculations were made for different values of the Peclet number, from 1 to 100, showing that the proposed method can be used for convection-dominated problems, as well as diffusive ones. Moreover, let us conclude by mentioning that in the case of very stiff boundary layers, a natural extension of the method would be to substitute a wavelet approximation to the Fourier approximation. The main advantage of using wavelets would be the possibility of using stretched grids, unlike the Fourier approximation which requires uniform grids.

ACKNOWLEDGMENTS

The calculations were made on the CRAY-YMP computer of the IMT (Marseille) with the support of region PACA.

REFERENCES

1. I. Manceau and D. Delaunay, ''Etude expérimentale et simulation des transferts de chaleur dans un moule d'injection de thermoplastiques,'' on *Proceedings, SFT Annual Congress*, 1993,'' p. 90.
2. B. L. Buzbee, F. W. Dorr, J. A. George, and G. H. Golub, *SIAM J. Num. Anal.* **8,** 722 (1971).
3. G. P. Astrakmantsev, *U.S.S.R. Comput. Math. Math. Phys.* **18,** 114 (1978).
4. M. Briscolini and P. Santangelo, *J. Comput. Phys.* **84,** 57 (1989).
5. C. Atamian, G. V. Dinh, R. Glowinski, J. He, and J. Periaux, *Comput. Methods Appl. Mech. Eng.* **91,** 1271 (1991).
6. R. Glowinski, T. W. Pan, J. Periaux, and M. Ravachol, ''A Fictitious Domain Method for the Incompressible Navier–Stokes Equations,'' in *Proceedings, The Finite Element in the 1990's*, edited by E. Onate, J. Périaux, and A. Samuelson (Springer-Verlag, Berlin, 1991), p. 410.
7. A. Garba, UNSA University thesis, 1993.
8. W. Borchers, F. K. Hebeker, and R. Rautmann, *in Notes of Numer. Fluid Mech.* edited by Hirschel (Vieweg, Braunscweig, 1986), p. 14.
9. H. Gründemann, *Eng. Anal. Boundary Elements* **6**(4), (1989).
10. C. Canuto, M. Y. Hussaini, A. Quarteroni, and T. A. Zang, ''Spectral Methods in Fluid Dynamics,'' in *Comput. Phys.* (Springer-Verlag, New York/Berlin, 1988).
11. C. A. Brebbia, J. C. F. Telles, and L. C. Wrobel, *Boundary Elements Techniques* (Springer-Verlag, New York/Berlin, 1984).
12. L. Schwartz, *Théorie des distributions* (Hermann, Paris, 1966).
13. F. Q. Hu, ICASE Report 94-15, 1994 (unpublished).
14. G. D. Baker and M. Shelly, *J. Comput. Phys.* **64,** 112 (1986).
15. R. Dautray and J. L. Lions, *Analyse mathématique et calcul numérique pour les sciences et les techniques*, Evolution: numérique, transport, Vol. 9 (Masson, Paris, 1988).
16. N. Nakagawa, *Eng. Anal. Boundary Elements* **13,** 383 (1993).